Available online at www.sciencedirect.com
ScienceDirect
Journal of Colloid and Interface Science 304 (2006) 518–523
JOURNAL OF Colloid and Interface Science
www.elsevier.com/locate/jcis

# Experimental humidity dependency of small particle adhesion on silica and titania

Matti Paajanen *, Jukka Katainen, Olli H. Pakarinen, Adam S. Foster, Jouko Lahtinen

*Laboratory of Physics, Helsinki University of Technology, P.O. Box 1100, FI-02015 TKK, Finland*

Received 24 June 2006; accepted 9 September 2006

Available online 14 September 2006

**Abstract**

The humidity present in ambient atmosphere affects the adhesion of small particles by causing capillary bridge formation between the particle and the surface. Even in moderate relative humidities this, usually attractive, force can have a significant effect on adhesion behaviour of micro and sub-micro particles. We have directly measured the pull-off forces of initially adhered oxide particles on oxide surfaces with atomic force microscope in controlled atmosphere with adjustable humidity. We demonstrate the effect of the surface roughness resulting in two different regions of capillary formation and the particle shape having a strong effect on the humidity dependency of adhesion. The experimental results are explained by theoretical framework.


*Keywords:* Capillary; AFM; Adhesion; Humidity

## 1. Introduction

Small particles adhere to surfaces due to the van der Waals interaction. Moisture changes the nature of this phenomenon and increases the adhesion of colloids to surfaces leading, e.g., to enhanced agglomeration of powders. This phenomenon is widely studied and is considered problematic in, e.g., pharmaceutical industry. There is a possible capillary meniscus formation between the bodies of interest in many systems, water being the most common liquid in normal conditions [1]. Similar effects might be found in systems with any vaporized substance.

The atomic force microscope (AFM) [2] has become very popular tool for various fields of science during the past 20 years. The ability to measure small forces and distances is utilized in multiple ways, e.g., in adhesion studies [3,4]. AFM studies often take place in ambient conditions with some humidity present, that can obscure the interpretation of the adhesion experiments, since the capillary force can be significant compared to other surface forces [1].

The capillary force between a small particle and surface has been measured with AFM by Mate et al. [5,6] using nonvolatile liquid films. The capillary force originating from the condensed water from ambient atmosphere has been shown to increase with humidity [7,8]. The surface roughness also plays a role in the capillary formation [9–12].

The modelling of the capillary force started very early with the standard approximation, for a review see, e.g., [1]. This humidity independent model was shown to be incorrect by Marmur [13] and further by de Lazzer et al. [14]. Ata et al. [11] present a model for capillary formation on a rough surface, where in low humidities the water meniscus appears between the particle and an asperity on the surface and in higher humidities the film extends to the planar surface below the asperity, as shown in Fig. 1. The calculation of the capillary forces between two spheres of unequal sizes has recently been done, e.g., by Rabinovich et al. [12]. The rigorous model described by Pakarinen et al. [15] includes any axially symmetric particle shape, although it is computationally more time consuming.

We have measured the humidity dependency of the pull-off force with spherical probes and truncated cones with AFM. We apply the model for the capillary force described by us [15] to the experimental results, using simplified meniscus shape, i.e.,

* Corresponding author. Fax: +358 9 451 3116.
*E-mail address:* matti.paajanen@tkk.fi (M. Paajanen).

0021-9797/$ – see front matter 
doi:10.1016/j.jcis.2006.09.017

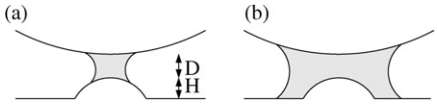


Fig. 1. Model for advancing meniscus formation on surfaces with finite roughness [11].

we assume a circular profile for the water meniscus. As shown previously [15] this makes an error less than 2% in the size scale of interest. In the experiments, we have discovered two humidity dependent regions, that can be nicely explained by our model using the two possible meniscus geometries of Fig. 1.

## 2. Experimental

### 2.1. AFM system

The experiments were performed with a Digital Instruments Nanoscope III atomic force microscope with extender electronics. The system is equipped with an atmospheric hood, which enables controlling the ambient atmosphere. The apparatus was used for force measurements as well as for surface imaging.

We used dry nitrogen (99.5%) gas to produce atmosphere with various humidity levels inside the hood. After introducing the sample and the probe, the atmosphere was dried by flowing dry nitrogen through the system. After drying the flow of nitrogen was reduced to amount sufficient to keep the relative humidity (RH) low (<5%) and constant. The humid gas was obtained using two-stage bubbler-type humidifier immersed in a heat bath. The dry and humid nitrogen were mixed to obtain the desired humidity. Humidity inside the hood was monitored using a Vaisala HMP233 humidity meter. The humidity was kept within RH 2% during each measurement point.

### 2.2. Surfaces and particles

The surfaces used in this study were a polished silicon wafer with native oxide and an atomic layer deposited (ALD) $TiO_2$ film [16,17]. The $TiO_2$ film was grown on borosilicate substrate at temperature of 620 K resulting in polycrystalline (anatase) film structure. Both surfaces were characterized using AFM imaging prior to the adhesion measurements. After filtering out the high frequency noise by a median filter, the asperity distributions were determined from the topographic AFM images by fitting a paraboloid on to each local maximum found on the 1 $\mu m^2$ image. The radius of the asperity is then obtained from the curvature of the fitted paraboloid. The height of the asperity is the difference between the maximum of the fitted parabola and the mean level of the grain border.

The radius and height distributions of our surfaces are shown in Fig. 2, where the mean asperity heights are $0.2 \pm 0.1$ and $0.9 \pm 0.5$ nm, and the radii of curvature $190 \pm 80$ and $50 \pm 30$ nm, for silica and titania, respectively. Although, these are only mean values, they give more information on the asperities than just the RMS roughness or some other single roughness parameter [18]. Contact angles were also measured by photographing the droplets on the surface resulting in 60° for silica and 80° for titania surface.

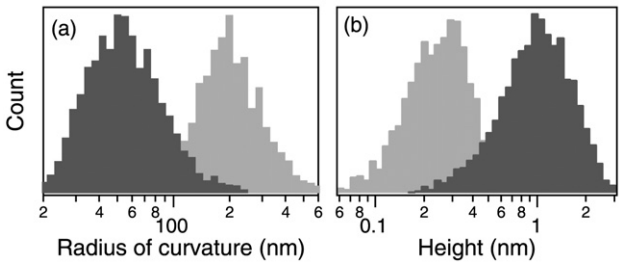


Fig. 2. Silica (light grey) and titania (dark grey) surface asperity (a) radius of curvature and (b) height distributions.

We used three types of model particles: sharp AFM probes as small particles (CSC17-F, Mikromasch and CONT, Nanosensors), silica spheres glued on AFM cantilevers (Novascan) as microspheres and eroded AFM probes as blunt particles. The blunt particles were made by eroding the fresh tips by scanning them in several directions against a silicon sample. Approximate scanning parameters were scan size 4 μm, rate 4 Hz, normal force 50 nN, and angles 0°, 45°, 90°, and 135°. The size of the flat area was controlled by the scanning time, though some variations on the normal force were also used. A set of sharp probes were also coated with titania using the ALD technique. We calibrated the force constants of all cantilevers using the Sader method [19], except the Mikromasch tips that were calibrated by the manufacturer using the same method.

### 2.3. Pull-off force measurements

The adhesion was measured using displacement–deflection curves obtained moving the sample toward and away from the probe and measuring the corresponding cantilever deflection as described earlier [3,20]. The loading, typically below 10 nN, was kept constant during measurements although the absolute value did not affect the pull-off forces. Each model particle was first used for a few hundred force measurements in dry $N_2$ atmosphere before the actual experiments since the pull-off force levelled off after an initial increase. When the humidity dependency was measured, the humidity was increased in RH 5–10% steps up to RH 80%. The humidity was then reduced in a few steps back to below 5% RH and the measurements were repeated in order to detect possible hysteresis between increasing and decreasing humidity. This would also reveal possible erosion of the probes during the measurements. We found no hysteresis nor erosion if the system was allowed to stabilize for about half an hour after any changes in the humidity.

In order to guarantee sufficient statistics, 100 displacement–deflection curves were recorded evenly distributed on an 1 $\mu m^2$ area. Two such sets of data were recorded on different locations on the surface. The measurements thus resulted in 200 displacement–deflection curves for each probe–surface–humidity combination covering 2 $\mu m^2$ of surface. The mean and standard deviation for each data set was calculated, and these values were used for further analysis.

The pull-off forces were extracted from the displacement–deflection curves by Perl scripts. The zero deflection was set to an average value of the retracting curve after the pull-off.

Lines were fitted to the contact part and the vertical pull-off part and the intersection of these lines with the zero deflection were used to calculate the distance the $Z$-piezo travelled before the pull-off. This distance was converted to force using the force constant of the cantilever. This indirect way to determine the pull-off force helps us to avoid the problems in photodiode calibration since the force is calculated from the $Z$ movement of the piezo tube alone.

## 3. Model for capillary forces

### 3.1. Capillary forces

The presence of water vapour in ambient environment causes capillary film formation between the particle and the surface in suitable conditions. The vapour pressure, $p$, determines the shape of the equilibrium water meniscus, characterized with the two radii of curvature, $r_1$ and $r_2$, as follows from the Kelvin equation [1]

$$\left(\frac{1}{r_1}+\frac{1}{r_2}\right)^{-1} = r_{\mathrm{K}} = \frac{\gamma V_0}{k_{\mathrm{B}} T \ln\frac{p}{p_{\mathrm{sat}}}}, \tag{1}$$

where $r_{\mathrm{K}}$ is the Kelvin radius, $p_{\mathrm{sat}}$ is the saturation vapour pressure, $\gamma$ is the surface energy of the liquid, $V_0$ is the mean volume of one water molecule, $k_{\mathrm{B}}$ is the Boltzmann constant, and $T$ is the temperature. Although, the sectional interface of the meniscus corresponding to the radius $r_1$ in Fig. 3 is not exactly circular, we have shown elsewhere [15] that circular profile assumption is valid in the size range where continuum modelling of water can be used.

The shape of the meniscus and its surface energy induce a pressure difference across the liquid/vapour interface [21]:

$$\Delta p = \frac{\gamma}{r_{\mathrm{K}}}. \tag{2}$$

The negative Laplace pressure, $\Delta p$, together with the direct surface tension make up the capillary force felt by the particle as additional adhesion force [15]

$$F = F_{\mathrm{p}} + F_{\mathrm{st}}, \tag{3}$$

$$F_{\mathrm{p}} = A_{\perp}\Delta p, \tag{4}$$

$$F_{\mathrm{st}} = l\gamma_{\perp}, \tag{5}$$

where $A_{\perp}$ is the horizontal projection of the wetted area, $\gamma_{\perp}$ is the vertical component of the surface tension, and $l$ is the length of the closed perimeter of the water meniscus at contact with the particle.

The water film not only causes additional capillary forces, but it also screens the van der Waals interaction. We include this effect by scaling the force measured in dry conditions with the ratio of water-mediated and vacuum-mediated Hamaker constants. The ratios used were 0.11 for silica [4] and 0.33 for titania [22] and 0.19 for $SiO_2$–$TiO_2$. The value for titania is for rutile, since no data for water mediated Hamaker constant for anatase was found. The $SiO_2$–$TiO_2$ value is obtained using the approximation $A_{12} = \sqrt{A_{11}A_{22}}$ [1].

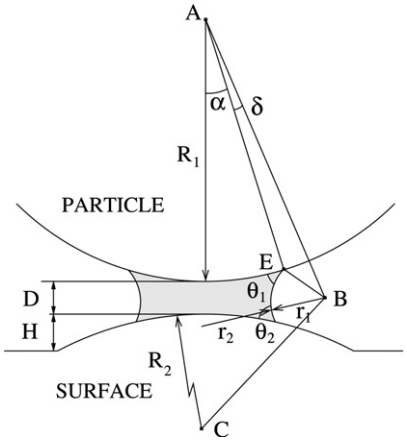


Fig. 3. Schematic diagram showing the meniscus formed between the particle and the surface.

### 3.2. Spherical particles

Using the geometry presented in Fig. 3, the capillary pressure force and surface tension force are obtained for a spherical particle as

$$F_{\mathrm{p}} = \pi(R_1\sin\alpha)^2\frac{\gamma}{r_{\mathrm{K}}}, \tag{6}$$

$$F_{\mathrm{st}} = 2\pi R_1\sin\alpha\gamma\sin(\alpha+\theta_1). \tag{7}$$

The filling angle $\alpha$ may be determined using $\theta_1$ and $\theta_2$ and radii $R_1$, $R_2$, and $r_1$. First expressions for the distances AB and BC can be derived using the cosine rule

$$\begin{aligned}|AB|^2 &= r_1^2 + R_1^2 - 2r_1R_1\cos(\pi-\theta_1)\\ &= r_1^2 + R_1^2 + 2r_1R_1\cos\theta_1,\end{aligned} \tag{8}$$

$$|BC|^2 = r_1^2 + R_2^2 + 2r_1R_2\cos\theta_2. \tag{9}$$

The distance BC can be written also using the triangle ABC and $\alpha+\delta$ as

$$\begin{aligned}|BC|^2 &= (R_1+R_2+D)^2 + |AB|^2\\ &\quad - 2|AB|(R_1+R_2+D)\cos(\alpha+\delta).\end{aligned} \tag{10}$$

Finally, the angle $\alpha$ is obtained by subtracting $\delta$ from $\alpha+\delta$, since $\delta$ can be solved from the triangle ABE.

In the case depicted in Fig. 1b Eq. (8) still applies, but the distance $|BC|$ has no meaning. The angle $\alpha+\delta$ can, however, be solved easily from the following equation (see Figs. 1 and 3)

$$R_1 + D + H = |AB|\cos(\alpha+\delta) + r_1\cos\theta_2 \tag{11}$$

and the angle $\alpha$ is obtained as above for the two sphere system. Equivalently, Eq. (11) is valid for a sphere above a planar surface when $H = 0$.

### 3.3. Blunt particles

The other particle shape we considered was a truncated cone. Using the geometry of Fig. 4 we can calculate the geometrical parameters $A_{\perp}$ and $l$ of Eqs. (4) and (5). The distance $x$ can be written as

$$x = (a+b)\tan\phi = r_1\big(\cos\theta_2 + \sin(\phi-\theta_1)\big)\tan\phi. \tag{12}$$

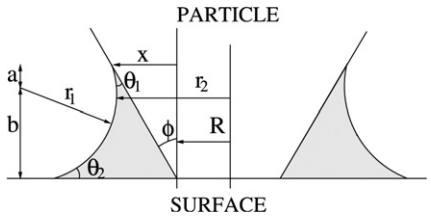


Fig. 4. Capillary bridge around a truncated cone on a flat surface.

Using the area of the wetted annulus we get for the vertical components of the pressure force and surface tension force

$$F_p = \pi\left(\frac{(x+R)^2 - R^2}{r_K}\right)\gamma, \tag{13}$$

$$F_{st} = 2\pi(R+x)\gamma\cos(\phi-\theta_1). \tag{14}$$

Another assumption made above is that, there is water directly between the particle and the surface, but it does not exhibit the same pressure as the water annulus around it. If the clearance $D$ between the particle and the surface is of the order of the size of a water molecule, the water between the surfaces cannot be considered as continuum and the pressure may vary from the value inside the water meniscus [15]. However, the screening of van der Waals forces through water is assumed as described above.

## 4. Results and discussion

### 4.1. Small particles

The measured pull-off forces for small silica particles on silica and titania surfaces as a function of humidity are presented in Fig. 5. Fig. 6 presents the same for titania coated particles. The measured series consist of three regions; humidity independent part below RH 20%, and two humidity dependent parts of advancing meniscus formation as shown in Fig. 1.

The experimental results were fitted to the model of Section 3.2. The geometrical parameters $R_2$ and $H$ were obtained from the topographical images of the surfaces. The calculation was performed by scanning through $r_1$ values and solving the corresponding $r_2$ values defined by $r_1$, geometry and contact angles. The relative humidity is then obtained from Eq. (1) and the force using Eqs. (6)–(11). The low and high humidity regions were calculated separately using appropriate geometries and the results are shown with dashed and solid lines in Figs. 5 and 6. Parameters used in the calculations are shown in Table 1. The sizes of the particles, $R_1$, were optimized to give the best fits to the experimental data. Some adjustments in other parameters were also needed, though they were kept inside their uncertainty limits. The value for particle–substrate separation $D$ was fixed to 0.25 nm.

For silica particles the model for the humidity dependency of the adhesion is very good. The shape of the force–humidity curves are nicely explained by the growth of the water meniscus between the particle and the surface as shown in Fig. 1. The difference in the optimal $R_1$ values for $SiO_2$ particles falls within the experimental error and agrees with the tip size obtained from scanning electron microscopy (SEM) images.

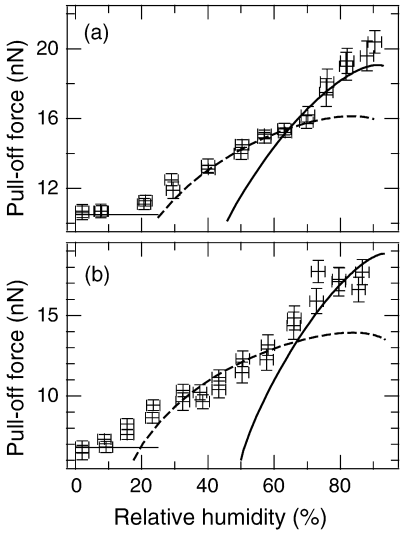


Fig. 5. Pull-off forces for small silica particles on (a) $SiO_2$ and (b) $TiO_2$ surface as a function of humidity. The dashed and solid lines represent theoretical humidity dependency with small and large water meniscus shown in Fig. 1.

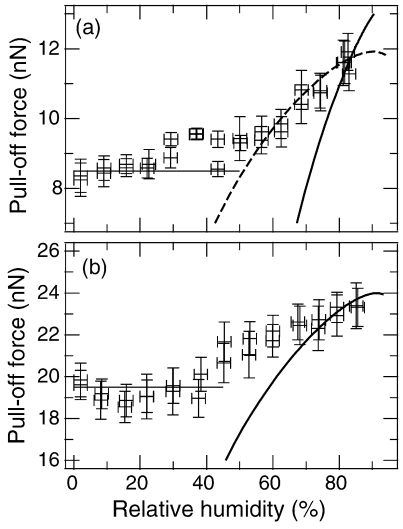


Fig. 6. Pull-off forces for small $TiO_2$ coated particles on (a) $SiO_2$ and (b) $TiO_2$ surface as a function of humidity. The dashed and solid lines represent theoretical humidity dependency with small and large water meniscus shown in Fig. 1.

The high contact angle on $TiO_2$ probes resulted in much less satisfactory agreement between the theory and the experiments for $TiO_2$ particles. For the $TiO_2$–$TiO_2$ system the low humidity curve could not be fitted at all. For small probes, the contact angle might be less than the value measured from the flat surface leading to similar agreement in the low humidity region as with silica spheres. We also had to use low asperity height $H$ for $TiO_2$ surface. This might result from the probes being smaller than the typical distance between the asperities causing the probe to fall to contact with a lower asperity in between the larger ones. Since the $TiO_2$ tips were coated silica tips, the larger radii are easily explained by the thickness of the coating.

The shape of the small probes is not exactly known, and can significantly differ from spherical. However, the assumed spherical shape gives reasonable results. In comparison with

Table 1
Parameters used in calculating the theoretical humidity dependencies for small particles

| Materials particle–surface | $R_1$ (nm) | $R_2$ (nm) | $\theta_1$ (deg) | $\theta_2$ (deg) | $H$ (nm) |
|---|---|---|---|---|---|
| $SiO_2$–$SiO_2$ | 35 | 140 | 0 | 60 | 0.27 |
| $SiO_2$–$TiO_2$ | 40 | 80 | 0 | 70 | 0.40 |
| $TiO_2$–$SiO_2$ | 45 | 200 | 70 | 60 | 0.30 |
| $TiO_2$–$TiO_2$ | 65 | – | 65 | 70 | – |

previous studies, the two humidity regions were also present in the studies by Ata et al. [11]. However, they do not observe humidity dependency inside these regions, only difference in the pull-off force between the two regions, probably due to unmatched sizes of the particle and the asperities.

### 4.2. Microspheres

The humidity dependency of the adhesion of silica microspheres on silica surface is shown in Fig. 7. Experimental data shows for both 1.0 and 2.5 μm spheres two regions; at low humidities the adhesion is constant and above RH 30% it starts to increase.

The solid lines in Fig. 7 represent the theoretical humidity dependence on flat substrate given by Eqs. (6)–(8) and (11). The best fit radii for the 1.0 and 2.5 μm spheres are 0.75 and 1.2 μm, respectively. Other parameters were $\theta_1 = 0°$, $\theta_2 = 60°$, and $D = 0.25$ nm. The calculated force–humidity curves seem to reproduce the measured data if the radii of curvature are assumed smaller than the radii determined from SEM images. It seems that the part of the sphere making the contact with the surface has some corrugation giving rise to a smaller local radius than that of the whole sphere.

The standard approximation [1] predicts that the adhesion force is independent on the relative humidity if the radius of spherical particle is larger than 1 μm and the particle–surfaces distance is zero. Neither particle used in this study satisfies the humidity independency, but they both exhibit similar humidity dependency as smaller particles. There is, however, only one humidity dependent region, because the particles are much larger than the surface asperities. The relative increase in the adhesion due to humidity is much weaker the larger the particle.

### 4.3. Blunt particles

For blunt silica particles we obtained humidity curves shown in Fig. 8. The computational forces are calculated using Eqs. (13) and (14) and assuming the absence of asperities both on the particle and on the surface. To obtain reasonable agreement, we fitted the parameters $R$ and $\phi$ in Fig. 4 resulting in $R = 14$ nm and $\phi = 75°$ for the smaller and $R = 28$ nm and $\phi = 81°$ for the larger particle. These values differ significantly from the nominal radii of 50 nm and 150 nm and half cone angle 10°–20° obtained using SEM, as shown in Fig. 9a for the larger blunt particle. Fig. 9b shows a section of a reverse AFM image of the same particle, obtained by scanning the probe over a reference grating with an array of sharp needles (TGT01, Mikromasch) resulting in an image of the probe instead of the grating. The SEM and reverse AFM images give the same information when they are scaled similarly. The contact angles and separation, $D$, were the same as for microspheres.

With blunt particles we expected much larger effect due to capillary formation since the radii of the flat tops after erosion were quite large. With a closer look on the reverse AFM images the flat tops were however slightly rounded as seen in Fig. 9b, and there might be enough room for capillaries to form between the particle and the surface, giving an effective radius of some tens of nanometres and half cone angles in the range of the fitted values.

The assumptions made in deriving Eqs. (13) and (14) seem to be justified: No continuum water film exists between the contact area of the particle and the surface, since the pressure force would increase the capillary force at least by a factor of 2. On the other hand, there obviously are water molecules between

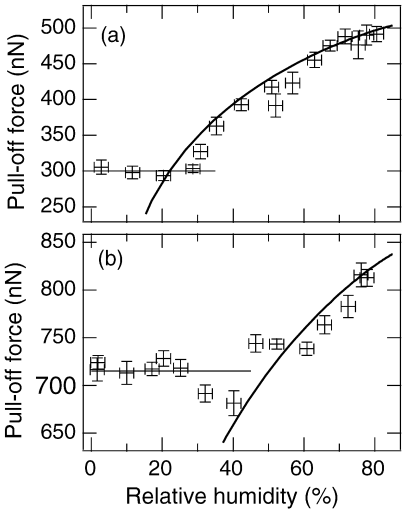


Fig. 7. Pull-off forces for silica microspheres on silica surface as a function of humidity: (a) $R_1 = 1.0$ and (b) 2.5 μm.

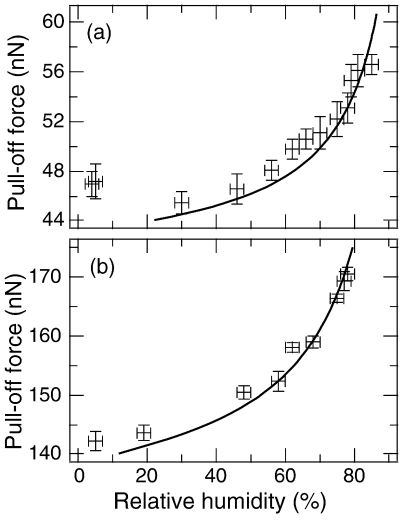


Fig. 8. Pull-off forces for blunt silica particles on silica surface as a function of humidity: (a) $R = 35$ and (b) 120 nm.

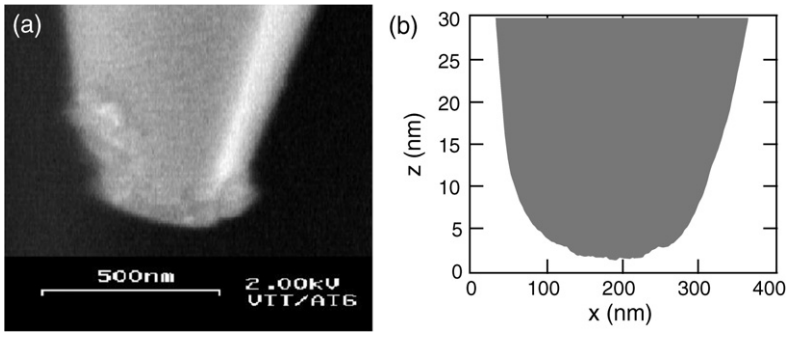


Fig. 9. The larger blunt particle: (a) a SEM image and (b) a section of a reverse AFM image. Note the scaling of (b).

the adhering surfaces screening the van der Waals interaction, since the absence of these would double the adhesion.

## 5. Conclusions

We have measured the humidity dependency of the adhesion with three types of particles. With small spherical particles the behaviour exhibit two regions, that can be explained by advancing meniscus formation first between the particle and an asperity and then between the particle and the surface. For micron sized spherical particles only the second type is detected. The blunt particles show only one humidity region, and the water layer directly between the particle and the surface is shown to screen the van der Waals force but not to mediate the hydrostatic pressure from the surrounding annular meniscus.

In the presence of experimental results, it is evident that the existence of the capillary force requires a certain threshold humidity. This is due to the instability of capillary film with very small radius of curvature as there are only few molecules to form the curved surface. Below RH $\sim$ 25% there is no continuum water to form a meniscus, and adhesion is not affected by capillary forces [8]. However, there might be effects due to monolayers of water on each object.

Present model for the effect of humidity explains well the experimental findings for different particle sizes and shapes. However, usage of parameters obtained from, e.g., SEM images may not result in correct estimates, since the phenomenon is very sensitive to local geometry, which may not be visible. Real applications often posses surface features covering many length scales, thus the correct parameters have to be selected carefully.

## Acknowledgments

The authors thank Ph.D. Janne Raula and Professor Esko Kauppinen at VTT for SEM images, M.Sc. Viljami Pore and Professor Markku Leskelä at University of Helsinki for ALD coatings. This work has been supported by the National graduate school of Materials Physics and the Finnish Funding Agency for Technology and Innovation (TEKES) via the PINTA Research Program.

## References

[1] J. Israelachvili, Intermolecular and Surface Forces, second ed., Academic Press, New York, 1992.
[2] G. Binning, C. Quate, C. Gerber, Phys. Rev. Lett. 56 (1986) 930.
[3] B. Cappella, G. Dietler, Surf. Sci. Rep. 34 (1999) 1.
[4] H.-J. Butt, B. Cappella, M. Kappl, Surf. Sci. Rep. 59 (2005) 1.
[5] C.M. Mate, M.R. Lorenz, V. Novotny, J. Chem. Phys. 90 (1989) 7550.
[6] C.M. Mate, V. Novotny, J. Chem. Phys. 94 (1991) 8420.
[7] C.M. Mate, M. Binggeli, Appl. Phys. Lett. 65 (1994) 415.
[8] X. Xiao, L. Qian, Langmuir 16 (2000) 8153.
[9] R. Jones, H.M. Pollock, J.A.S. Cleaverand, C.D. Hodges, Langmuir 18 (2002) 8045.
[10] Y.I. Rabinovich, J.J. Adler, M.S. Esayanur, A. Ata, R.K. Singh, B.M. Moudgil, Adv. Colloid Interface Sci. 96 (2002) 213.
[11] A. Ata, Y.I. Rabinovich, R.K. Singh, J. Adhes. Sci. Technol. 16 (2002) 337.
[12] Y.I. Rabinovich, M.S. Esayanur, B.M. Moudgil, Langmuir 21 (2005) 10992.
[13] A. Marmur, Langmuir 9 (1993) 1922.
[14] A. de Lazzer, M. Dreyer, H. Rath, Langmuir 15 (1999) 4551.
[15] O.H. Pakarinen, A.S. Foster, M. Paajanen, T. Kalinainen, J. Katainen, I. Makkonen, J. Lahtinen, R.M. Nieminen, Model. Sim. Mat. Sci. Eng. 13 (2005) 1175.
[16] M. Leskelä, M. Ritala, Thin Solid Films 409 (2002) 139.
[17] V. Pore, A. Rahtu, M. Leskelä, M. Ritala, T. Sajavaara, J. Keinonen, Chem. Vap. Deposit. 10 (2004) 143.
[18] J. Peltonen, M. Järn, S. Areva, M. Linden, J.B. Rosenholm, Langmuir 20 (2004) 9428.
[19] J.E. Sader, J.W. Chon, P. Mulvaney, Rev. Sci. Instrum. 70 (1999) 3967.
[20] W.A. Ducker, T.J. Senden, R.M. Pashley, Langmuir 8 (1992) 1831.
[21] F.M. White, Viscous Fluid Flow, second ed., McGraw–Hill, New York, 1991.
[22] H.D. Ackler, R.H. French, Y.-M. Chiang, J. Colloid Interface Sci. 179 (1996) 460.